J Appl Electrochem (2010) 40:1671–1681
DOI 10.1007/s10800-010-0163-1

ORIGINAL PAPER

Effect of current density and electrolyte concentration on hillock growth from pure bright Sn electrodeposits

K.-W. Moon · S.-K. Kim · M. E. Williams · W. J. Boettinger · G. R. Stafford

Received: 9 October 2009 / Accepted: 12 June 2010 / Published online: 1 July 2010
© U.S. Government 2010

Abstract The effect of current density and Sn methane sulfonate concentration on hillock density, columnar grain size, crystallographic texture, and residual stress of bright Sn electrodeposits is measured. Correlation was found between hillock density and the ratio of the applied current density to the transport limited current density. When the ratio exceeds unity no hillocks are observed. As the transport limited current is approached and exceeded, the columnar grain size decreases from 1.4 to 0.7 µm and the preferred orientation (fiber texture) rotates toward the [001] direction. Possible explanations are presented for how these factors reduce hillock growth. Because hillock and whisker growth are related phenomena, electrodeposition beyond the limiting current may be a possible whisker mitigation strategy.

Keywords Hillocks · Sn whiskers · Pb-free solder · Electrodeposition · Texture · Preferred orientation · Stress

1 Introduction

The introduction of Pb-free surface finish technology into electronic packages has renewed interest in Sn whisker growth. Sn whiskers can grow from electrodeposits spontaneously [1], during storage or service [2], often causing short circuits in pre-tinned electronic components. They appear to be a local response to the presence of compressive residual stress [3]. There are many proposed sources of the compressive residual stress: intermetallic compound (IMC) formation due to the reaction of Sn and Cu in the substrate metal [4–8], intrinsic plating stress [9], precipitation of IMC within the supersaturated Sn solid solution produced when Cu^{2+} is present in the electrolyte [9] and oxidation [10].

There are various types of surface defects on Sn and Sn alloy electrodeposits: whiskers, odd-shape eruptions, and hillocks. Typically, whiskers and odd-shape eruptions are observed when the grain boundaries of the Sn electrodeposit appear to be immobile (e.g., Sn–Cu deposits) while hillocks are observed when the grain boundaries are mobile (e.g., pure Sn deposits) [9]. The whiskers/hillock growth mechanism is diffusional grain boundary creep that feeds material to the base of the whisker/hillock grain [9, 11–13]. The columnar structure typical of many electrodeposits exacerbates the whisker problem. Pb additions breakup columnar structures into equiaxed structures that enable a more uniform creep response in the deposit interior to relieve stress [9]. Despite the knowledge gained through recent research, further study of the effect of deposition conditions on the deposit microstructure of Sn is needed.

In the present study we evaluate the effect of current density and the Sn^{2+} concentration in the electrolyte. We employed the rotating disk electrode method to obtain uniform mass transport in a reproducible manner. In particular we investigate situations that include transport limited growth at less than full plating efficiency.

K.-W. Moon · M. E. Williams · W. J. Boettinger (✉) · G. R. Stafford
Metallurgy Division, National Institute of Standards and Technology, 100 Bureau Drive, Gaithersburg, MD 20899-8555, USA
e-mail: william.boettinger@nist.gov

S.-K. Kim
Center for Fuel Cell Research, Korea Institute of Science and Technology, 39-1 Hawolgok-dong, Seongbuk-gu, Seoul 136-791, South Korea

2 Experimental

2.1 Substrates for electrodeposition

For the measurement of microstructure, preferred grain orientation and hillock density, 99.998% (mass) pure rolled Cu substrates, 2.5 cm square and 500 µm thick were employed. For the measurement of stress, cantilever beam coupons were fabricated in the geometry shown in Fig. 1 using electrical discharging machining of a stack of 125 µm thick, half hard, rolled phosphor bronze coupons (yield strength midway between fully annealed and fully cold worked). Phosphor bronze was employed in lieu of pure Cu because of the difficulty in preparing thin sheets in the cantilever geometry. The nominal mass fractions of phosphor bronze are Cu–5% Sn–(0.03% P–0.35% P). The cantilever beam direction was perpendicular to the sheet rolling direction to obtain reproducible beam deflections of electrodeposits.

Prior to plating, both sides of the substrates were polished with 3 µm diamond paste and finished on the surface to be plated with 1 µm diamond paste. All substrates were further cleaned in a 25% sulfuric acid solution for 30 s and rinsed in alcohol and deionized water. Samples were weighed and attached to the bottom of a rotating disk electrode assembly with plating tape so that deposition was restricted to one side of the coupon or cantilever. On the pure Cu coupons, a mask was employed to create a circular deposit area of 3 cm^2 whereas on the cantilever coupons, a mask was employed to expose only the central beam portion of the coupon.

2.2 Electrodeposition

To enable reproducible hydrodynamics, a rotating disk electrode assembly was used at 200 revolutions per minute (rpm). Plating was performed at 25 ± 0.5 °C. The Sn anode was a 99.999% sheet positioned beneath the rotating disk so that the working and counter electrodes were parallel. Preliminary experiments estimated the plating efficiency, so that plating times were adjusted to maintain a deposit thickness close to 15 µm for all samples. After plating, the plating tape was dissolved with acetone, and the samples were rinsed with deionized water.

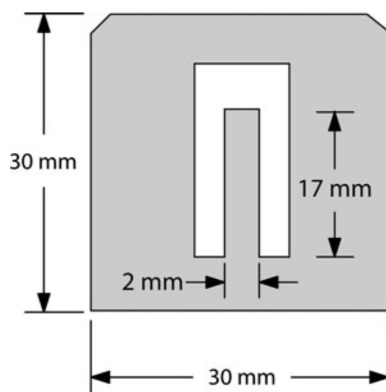

Fig. 1 Schematic of cantilever beam geometry used for post-deposition stress measurement. Only one side of the center tongue is plated

Three sets of samples were prepared on the pure Cu substrates with the plating conditions shown in Fig. 2. Electrolytes for bright Sn deposition were prepared from generic 70% methane sulfonic acid (MSA) and Sn^{+2} methane sulfonate (300 g L^{-1} concentration) with Sn^{+2} concentrations between 0.24 and 0.57 mol L^{-1} by diluting with high purity water with a resistivity of 18.3 MΩ cm. Commercial isopropanol based leveler and brightener were added at the rate of 120 and 20 mL L^{-1}, respectively. The current densities were between 20 and 200 mA cm^{-2}. The first data set (Exp-1) was performed at a fixed concentration of 0.38 mol L^{-1} and the current density was varied. The second and third sets (Exp-2 and Exp-3) were performed with different but constant ratios of Sn^{2+} concentration to current density. Following the analysis of Levich [14] for the rotating disk electrode, the limiting current density is given by

$$i_{l,c} = 0.62nFD^{2/3}\omega^{1/2}\upsilon^{-1/6}C^* \quad (1)$$

where nF is the charge transferred per mole of Sn^{2+} (C mol^{-1}), C^* is the Sn^{2+} concentration in the electrolyte, D is the diffusion coefficient for Sn^{2+}, ω is the angular rotation rate of the electrode in radians s^{-1}, and υ is the kinematic viscosity. Thus the experiments of Exp-2 and Exp-3 were designed to be conducted at different but fixed ratios of current to limiting current $i/i_{l,c}$. Fig. 2 shows the current density and Sn^{2+} concentration used for the three experimental conditions as well as the diffusion limited current calculated from Eq. 1 assuming that D equals 3.84 × 10^{-6} cm^2 s^{-1} and that υ equals 0.01 cm^2 s^{-1} (the value for D was calculated from data that will be presented later in the paper). It is clear from Fig. 2 that the deposition currents for Exp-1 span the range from below to above the diffusion limited current for Sn deposition. The Exp-2 condition was chosen to operate near but not exceed the limiting current so that the surface concentration of Sn^{2+} is close to zero, whereas the Exp-3 condition was well below the limiting current so that the Sn^{2+} surface concentration is close to the bulk value.

2.3 Measurement methods

The plating efficiency was calculated from the difference of sample weight between pre-deposit and post-deposit as the ratio between the actual amounts of metal deposited to that calculated theoretically from the charge passed using Faraday's law with 1 µm of Sn requiring a charge density

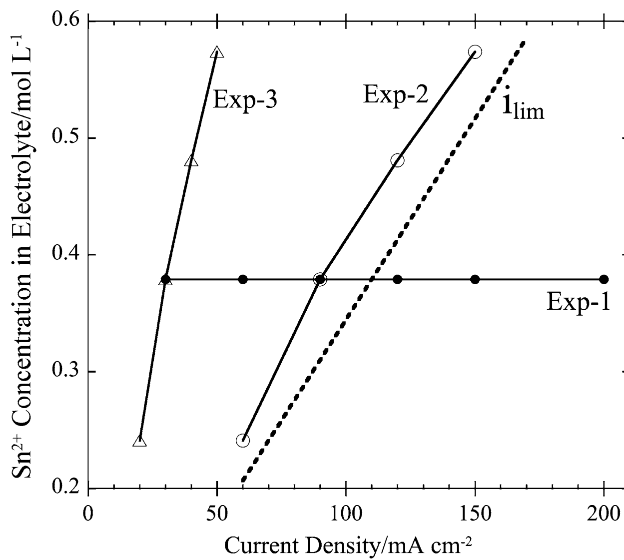

Fig. 2 The points summarize the three experimental data sets performed. The *dashed line* represents the diffusion-limited current density, calculated from Eq. 1 where $D = 3.8 \times 10^{-6}$ cm^2 s^{-1}, $\omega = 20.9$ rad s^{-1} (200 rpm), and $\upsilon = 0.01$ cm^2 s^{-1}

of 1.2 C cm^{-2}. The sample surfaces were examined using scanning electron microscopy (SEM). Selected samples were surface cleaned and/or cross-sectioned by focused ion beam (FIB) to examine the deposit grain shape on the surface and in the interior of the deposit. The improved contrast between grains obtained with channeling images taken in the FIB were found useful to identify some ambiguous grain boundaries seen in the SEM images. The surface grain size was obtained by the line/intercept method. The lines were constructed as a 13 × 9 grid.

The hillock density was determined after 127 days of room temperature storage by averaging densities from 15 SEM photographs (126 μm × 88 μm) taken at five locations from center to edge (with 4 mm gap) and three different positions normal to the radial direction (1 mm gap). As described in a previous study [9] using similar conditions, only hillocks were observed in pure Sn electrodeposits, not whiskers. Hillocks form when the grain boundaries of the deposit are mobile, whiskers form when they are pinned, but both grow due to a diffusion mechanism to relieve compressive stress. Thus a study of hillock density can yield information useful for whisker mitigation.

To determine initial stresses in the deposits, cantilever samples of phosphor bronze were plated with Sn under the conditions of Exp-1. The deflection of the cantilever beams was measured using an optical microscope from the change in focal position of the beam tip compared to the frame of the coupon. The measurement was performed within 15 min of plating. These measurements were performed with the coupon horizontal in the two orientations with respect to gravity. Correction to the deflection was made

Table 1 Parameters for Stoney's equation and other mechanical parameters

$E_s' =$ Substrate biaxial modulus $= E_s/(1 - \nu_s) = 216$ GPa, ($E_s = 134$ GPa, $\nu_s = 0.386$) [9]
$d_s =$ Substrate thickness = 125 μm
$d_f =$ Deposit thickness = 15 μm
$L =$ Beam length = 17 mm
$\delta =$ Deflection of beam from position prior to plating

for the thickness of the beam due to plating. The position of the beam was taken as the mean of the measurements. The change in position from the initial position (prior to plating) is defined as the deflection. The average stress was calculated using the thick deposit form of Stoney's equation,

$$\sigma_f = \frac{E_s'}{3}\frac{d_s^2}{d_f}\frac{\delta}{L^2}\left[1 - \frac{d_f}{d_s}\right] \quad (2)$$

where the notation is defined in Table 1. The stress values reported are the average of two or three samples for each current density.

Due to the rotation of the sample during deposition, the preferred grain orientation (PF) was assumed to be a fiber texture and was evaluated from the peak intensity of X-ray (theta-two theta) diffraction (XRD) data taken from the samples. Using Cu K_α radiation, diffraction peaks between 30° and 135° of 2θ were employed. The results are expressed in terms of a Preferred Orientation Factor, *PF*(*hkl*), which is defined [15] as:

$$PF(hkl) = \frac{I(hkl)/I_0(hkl)}{\frac{1}{n}\sum_n I(hkl)/I_0(hkl)} \quad (3)$$

where $I(hkl)$ is the measured intensity of *hkl* reflections, $I_o(hkl)$ is the intensity of *hkl* reflections for a random powder, and n is the number of reflections included in the analysis. A value of the *PF(hkl)* larger than one indicates that the (*hkl*) plane normal are more likely to be perpendicular to the surface of the electrodeposit than in a random grain structure sample.

3 Results

3.1 Plating efficiency

Figure 3a shows the average deposit growth rate, calculated from the deposit mass vs. current density for the three sets of data. The dashed straight line represents the growth rate calculated for the deposition current densities assuming that Faraday's law applies. The fact that the Exp-2 and Exp-3 follows the calculated growth curve confirms that

the applied current density is lower than the limiting current density, as expected from Fig. 2. The Exp-1 data set, at fixed Sn^{2+} concentration, shows a lack of linearity indicating that growth becomes diffusion limited at high current density. Ideally, one would expect the Exp-1 data to follow the calculated curve up to the diffusion-limited current, at which point the growth rate would remain constant. The gradual increase in growth rate, up to the maximum value of 92 nm s^{-1}, is likely due to non-uniform current distribution on the disk electrode; the periphery of the disk generally has a slightly higher current density than the center. A growth rate of 92 nm s^{-1} corresponds to a deposition current density of 110 mA cm^{-2}. Taking this value as the limiting current for the Exp-1 data allows us to calculate a Sn^{2+} diffusion coefficient of 3.84×10^{-6} cm^2 s^{-1} from Eq. 1, assuming the kinematic viscosity of the electrolyte is 0.01 cm^2 s^{-1}. This value is somewhat smaller than the 6.6×10^{-6} cm^2 s^{-1} value reported in a similar study of Sn^{2+} in MSA electrolyte [16]. Figure 3b gives the same results plotted as the more sensitive measure, current efficiency vs. current density, with slight deviations from the above described behavior being apparent. The Exp-2 and Exp-3 data sets have efficiencies near 100% while the efficiency for Exp-1 drops to 54% at 200 mA cm^{-2}.

3.2 Microstructures

Figure 4 shows FIB images of the as-deposited surface and cross-section of selected Exp-1 deposits. The cross sectional images clearly show that the grains are columnar and that increasing the current density results in a finer columnar grain diameter. Figure 5 shows portions of the larger field of view used for quantitative grain size determination. Other interesting features are also observed. For example, the sample at 30 mA cm^{-2} applied current density shows a ridged or undulating top surface morphology within some of the grains (Fig. 5a) whereas the surface morphology is smoother at higher currents. Many grain boundaries (observed as they intersect the top surface) are wavy rather than being straight for the lower current samples. No micro-pores as might be formed by hydrogen evolution at the higher currents were observed. SEM images of the as-deposited Exp-2 and Exp-3 surfaces are shown in Fig. 6 and 7. Little change in the overall columnar grain diameter is observed with increasing current density for these two series where the electrolyte composition is adjusted in order to maintain the same ratio of Sn^{2+} concentration to current density. We also note that the entire series for Exp-3 possess the same ridged or undulating top surface morphology in some grains as shown at the lowest current sample in series Exp-1. It is interesting to note that these Exp-3 deposits and the low

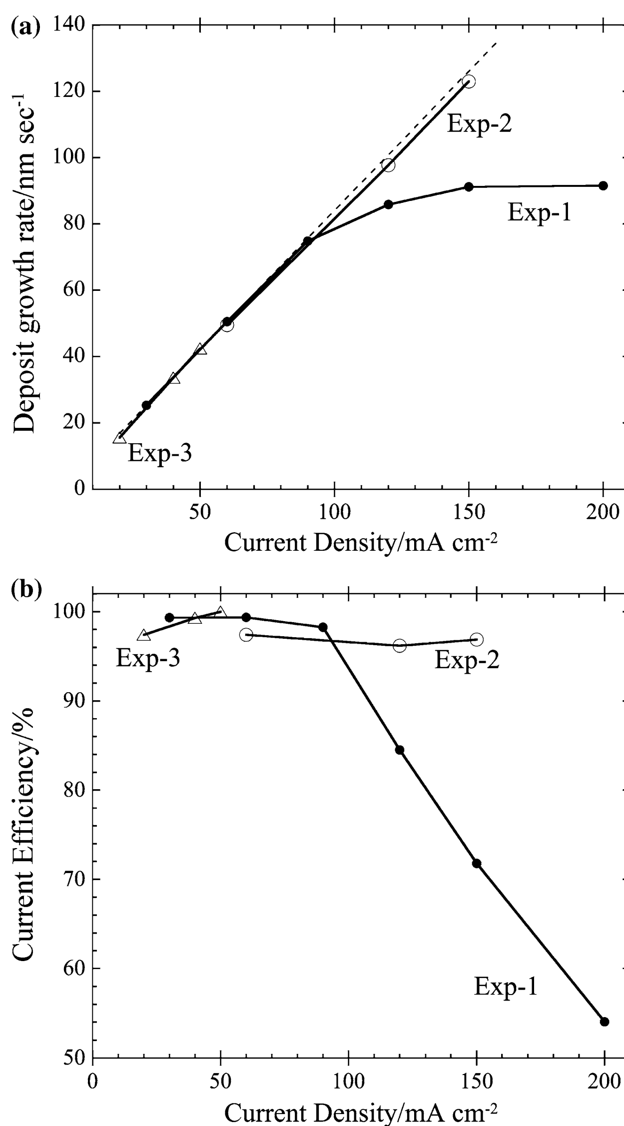

Fig. 3 **a** Deposit growth rate and **b** current efficiency versus current density for the three data sets

current Exp-1 deposits that posses this ridged surface morphology have the same (332) orientation (presented later), suggesting that crystallographic texture may be responsible for this surface morphology.

Figure 8 is a plot of the columnar grain diameter for all three data sets for these bright Sn deposits as a function of current density. As seen in the FIB images, the grain size of the Exp-1 deposits decreases significantly with increasing current density whereas those of both the Exp-2 and Exp-3 deposits show a very slight increase. We attribute this slight grain size increase to a slight decrease in the brightener concentration as a consequence of Sn MSA addition while making the more concentrated solutions. Electrodeposition involves a competition between nucleation and growth and a large number of variables in the

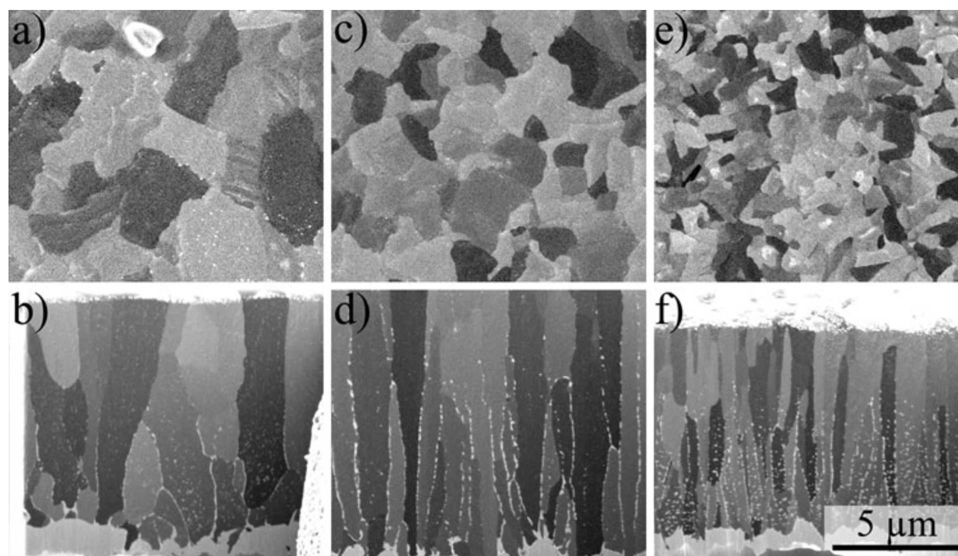

Fig. 4 Ion channeling images produced in the FIB for three of the Exp-1 data set; surface microstructures (**a**, **c**, **e**) and cross section microstructures (**b**, **d**, **f**); current densities: **a** and **b** 30 mA cm^{-2}, **c** and **d** 90 mA cm^{-2}, and **e** and **f** 200 mA cm^{-2}. The *white* speckle in (**b**, **d**, **f**) is an artifact of ion milling

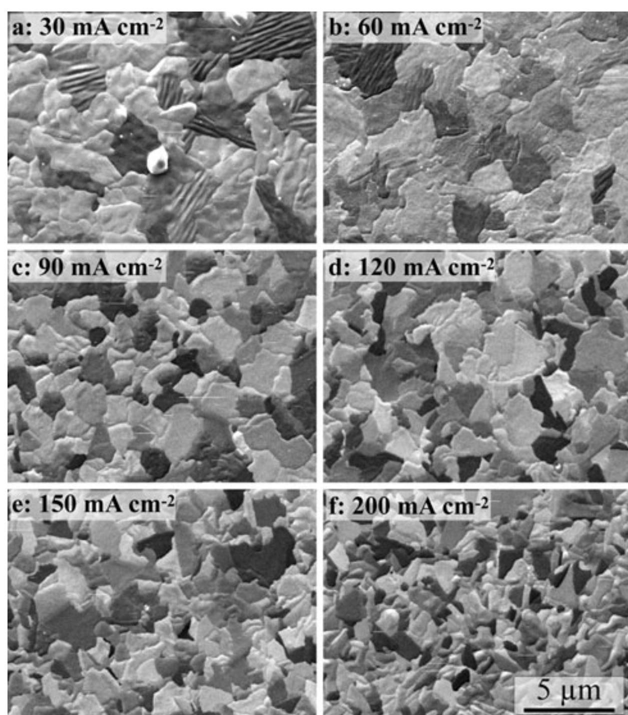

Fig. 5 Ion channeling images produced in the FIB for the top surface for all of the Exp-1 data set (see Fig. 2) in order of increasing current density

plating process influence deposit microstructure. Experimentally it is generally observed that increasing the deposition current (or deposition overpotential) favors nucleation, which results in grain refinement. Smaller grains are also favored when the electroactive metal ion concentration is reduced [17]. These experimental observations are supported by fundamental treatments developed from the viewpoint of nucleation theory [18–20] where an increased overpotential leads to a finer grain size. For Ni a decrease in grain size with increasing current density has been observed and modeled [21].

3.3 Preferred orientation of deposit growth

The X-ray diffraction patterns are shown in Fig. 9a for Exp-1 and in Fig. 9b for the additional samples from Exp-2 and Exp-3. From these data the preferred orientation factors for all three data sets are plotted vs. current density in Figs. 10, 11, 12. Starting with the Exp-1 data set, there are three clear texture regimes as the current density is increased to and beyond the diffusion limited value. At low current density, the deposits show strong texture for Sn(332) and Sn(312). As the current density approaches the limiting current the preferred orientation changes to Sn(011) and Sn(323). Beyond the limiting current, where hydrogen is evolved, the Sn(112) and Sn(123) orientation is favored. The change in orientation is summarized in Fig. 13.

The other two data sets show similar texture behavior to that observed in the Exp-1 data. The Exp-2 data which operated near the limiting current shows strong Sn(011) and Sn(323) texture, similar to that observed in Exp-1 as the deposition current approaches the limiting current. The Exp-3 data set which is limited to current densities well below the diffusion-limited current shows strong Sn(332) and Sn(312) texture, similar to the Exp-1 data at low current density. This is best summarized again in Fig. 13. The preferred orientations grouped furthest from the (001) pole (dark symbols) are consistent with deposition currents that are well below the diffusion-limited current, where the surface concentration of Sn^{2+} is close to the bulk value. The next group of preferred orientations (gray symbols) is consistent with deposition near the limiting current while the final group (open symbols) is associated with deposition

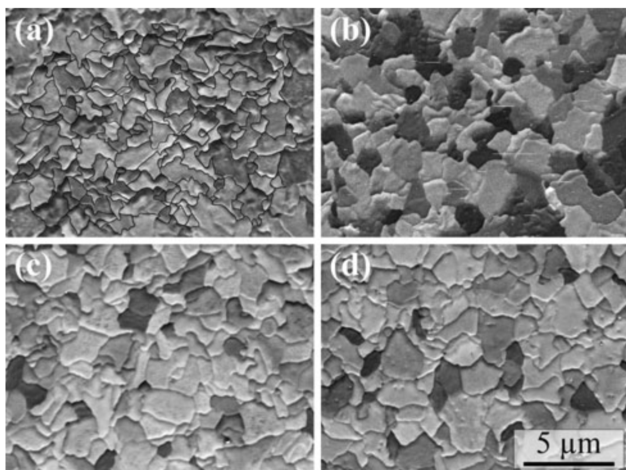

Fig. 6 SEM surface microstructures of Exp-2: **a** 60 mA cm^{-2} and 0.24 mol L^{-1} of Sn^{2+}, **b** 90 mA cm^{-2} and 0.38 mol L^{-1} of Sn^{2+}, **c** 120 mA cm^{-2} and 0.48 mol L^{-1} of Sn^{2+}, and **d** 150 mA cm^{-2} and 0.57 mol L^{-1} of Sn^{2+}. Due to the surface undulations in **a**, the outlines of some of the grain boundaries are drawn in *black*

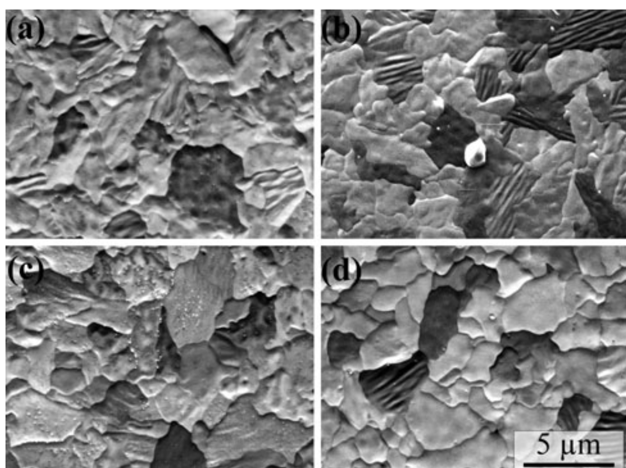

Fig. 7 SEM surface microstructures of Exp-3: **a** 20 mA cm^{-2} and 0.24 mol L^{-1} of Sn^{2+}, **b** 30 mA cm^{-2} and 0.38 mol L^{-1} of Sn^{2+}, **c** 40 mA cm^{-2} and 0.48 mol L^{-1} of Sn^{2+}, and **d** 50 mA cm^{-2} and 0.57 mol L^{-1} of Sn^{2+}

at currents that exceed the limiting current; i.e., significant hydrogen evolution occurs. The general behavior for all of the data sets suggests that as i/i_{lim} increases, the crystallographic texture favors a (001) orientation.

3.4 Initial stress

Figure 14 shows the stress measured immediately (15 min) after deposition vs. the current density for Exp-1. All samples show compressive stress. The compressive stress of the different samples increases as the current density increases up to 150 mA cm^{-2}, and then decreases or at least levels off. As shown in Fig. 3b, the plating efficiency

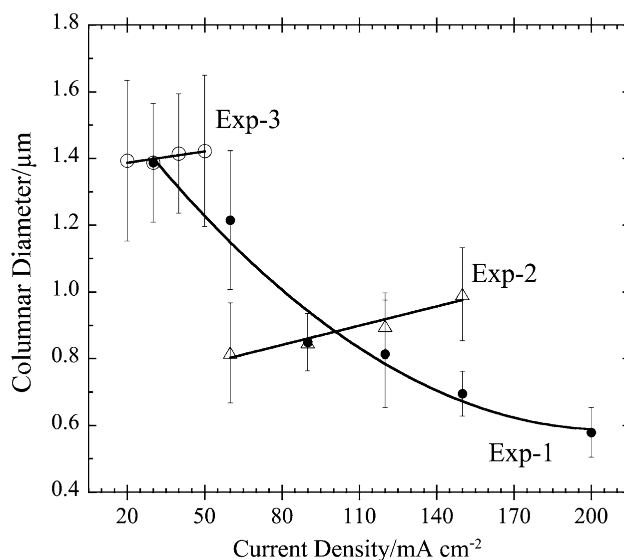

Fig. 8 Columnar grain diameter versus current density for three data sets

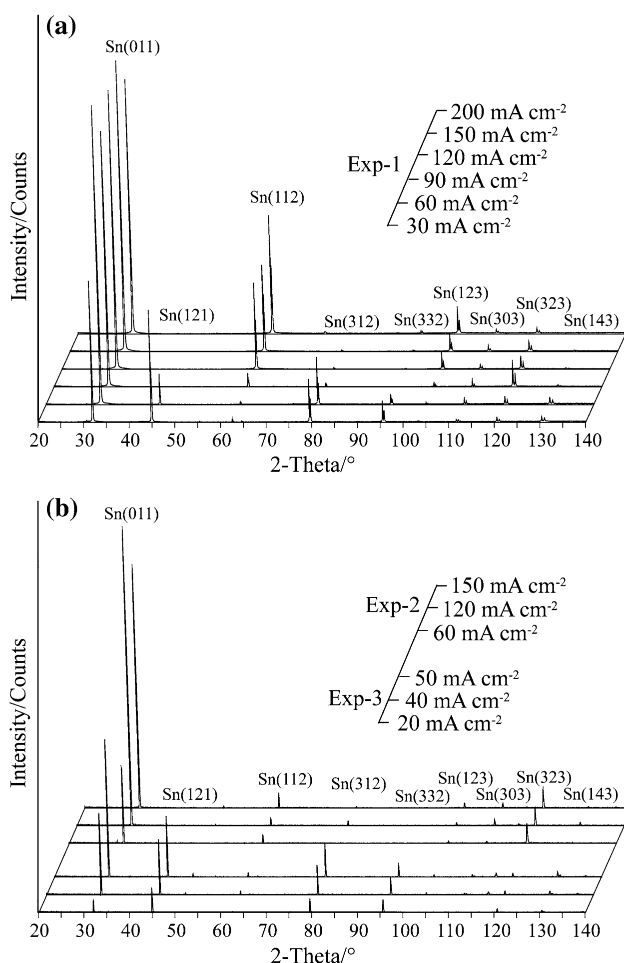

Fig. 9 Diffraction patterns of Sn deposits: **a** Exp-1; **b** Exp-2 and Exp-3

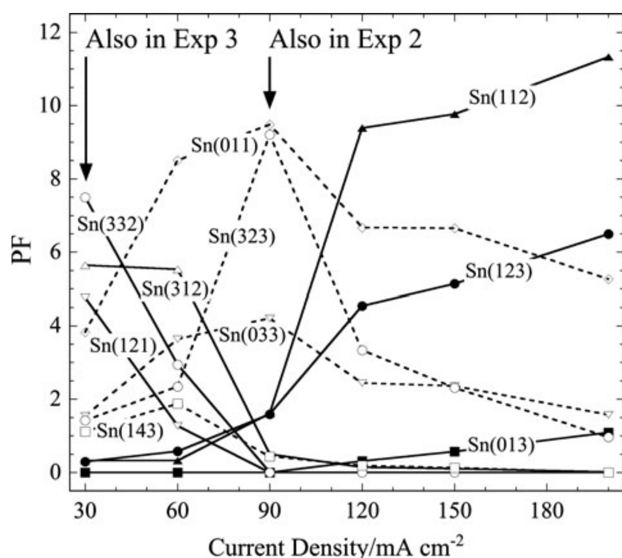

Fig. 10 Preferred orientation factor (PF) for various (hkl) reflections versus current density of Exp-1

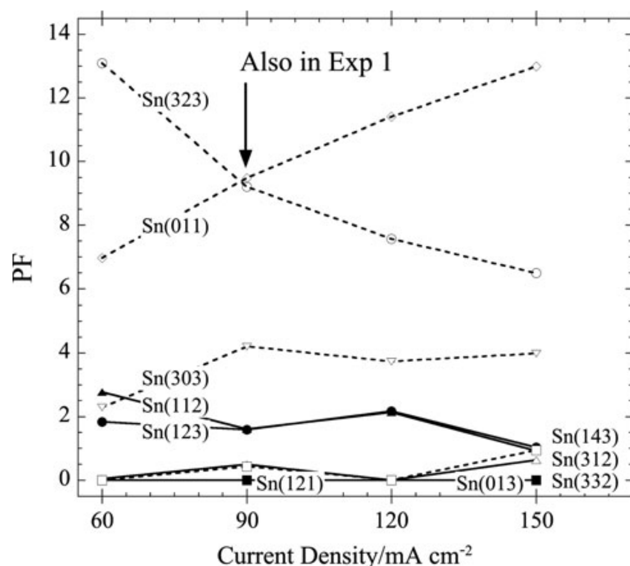

Fig. 11 Preferred orientation factor (PF) versus current density of Exp-2. Note that Sn^{2+} concentrations in electrolytes are varied as 60 mA cm^{-2} and 0.24 mol L^{-1} of Sn^{2+}, 90 mA cm^{-2} and 0.38 mol L^{-1} of Sn^{2+}, 120 mA cm^{-2} and 0.48 mol L^{-1} of Sn^{2+}, and 150 mA cm^{-2} and 0.57 mol L^{-1} of Sn^{2+}

is significantly reduced above 90 mA cm^{-2}. The actual thicknesses, designed to be near 15 μm and determined by weight gain after plating, are given in parentheses. Even though we employ different substrate material for the stress measurement, differences due to the diffusional interaction of substrate and deposit are at a minimum at a time of 15 min after plating. In addition we observe no significant differences in surface microstructure, preferred growth orientation and hillock formation from those plated on pure

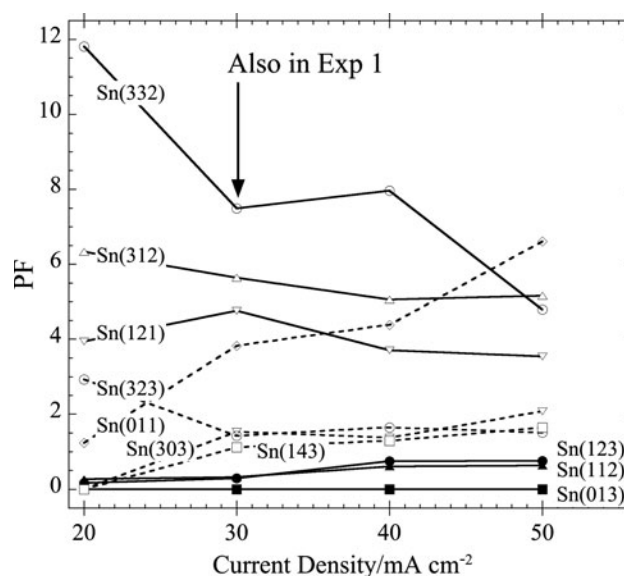

Fig. 12 Preferred orientation factor (PF) versus current density of Exp-3. Note that the Sn^{2+} concentrations in electrolytes are varied 20 mA cm^{-2} and 0.24 mol L^{-1} of Sn^{2+}, 30 mA cm^{-2} and 0.38 mol L^{-1} of Sn^{2+}, 40 mA cm^{-2} and 0.48 mol L^{-1} of Sn^{2+}, and 50 mA cm^{-2} and 0.57 mol L^{-1} of Sn^{2+}

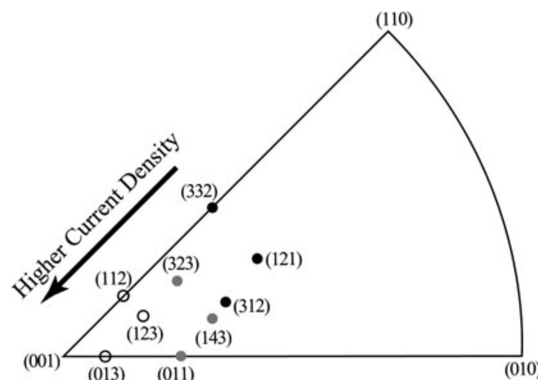

Fig. 13 The *dark*, *gray* and *open symbols* triplets indicate the planes with the highest preferred orientation factors as the current density increases. Data is for Exp-1 with a fixed concentration of 0.38 mol L^{-1} of Sn^{2+}

Cu. Thus, we assume that the stress measured at early time using the phosphor bronze cantilevers correctly gives the stress level of the Sn deposits on the pure Cu coupons.

3.5 Hillock density

The average hillock density was measured 127 days after deposition. Typical SEM views of the surface are shown in Fig. 15 and the density vs. deposition current is shown in Fig. 16. The hillock density is reduced in all three data sets with increasing current density. In Exp-1, no hillocks are observed when the applied current density is 120 mA cm^{-2} or above; i.e., when the current efficiency drops below

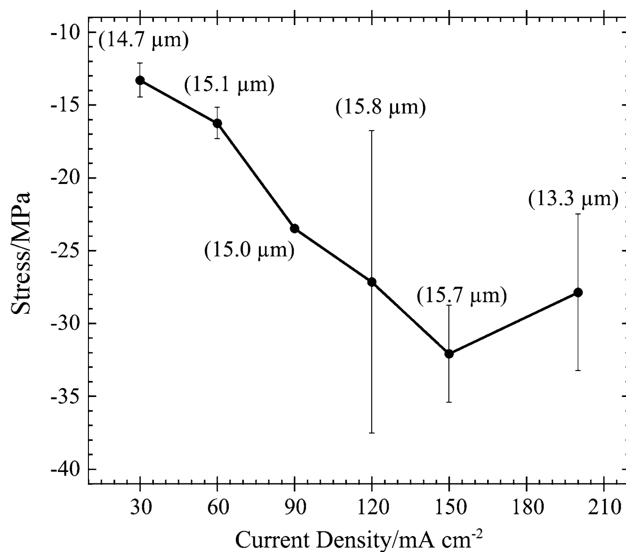

Fig. 14 Stress measured 15 min after plating versus current density for the Exp-1 series. The value in the *parenthesis* gives the actual deposit thickness as it varied from the targeted 15 µm value. The error bars show the range of measured values of stress

100%. Hydrogen evolution was only observed for Exp-1 above 120 mA cm^{-2}. The hillock density is generally low for Exp-2, a set that was designed to operate near the conditions of the diffusion limit. The Exp-3 set, far from the diffusion limit, has a high hillock density. When hillocks occur, they can be observed under an optical microscope growing within a minute of withdrawal from the plating bath. Their rapid growth is consistent with our measurement herein that compressive stress exists immediately upon plating and is due to the plating process itself. Additional compressive stress is added at a much slower rate due to intermetallic formation [9]. We report the hillock density after 127 days to show the effect of both sources of stress.

4 Discussion

We have investigated the effect of plating current and electrolyte concentration on the tendency to form hillocks in pure Sn electrodeposits. We have found that when plating conditions exceed the limiting current for diffusive transport of Sn ions through the hydrodynamic boundary layer that the hillock density can be reduced to zero. This reduction is in spite of the fact that the compressive stress measured in the deposits remains quite high and the grain structure remains relatively columnar. Both of these factors have been thought to increase the likelihood of hillock and/or whisker formation. Below we discuss the various issues in turn that may play a role in these results.

4.1 Hydrogen evolution

Our results show reduced hillock formation as the plating efficiency decreases. Thus a discussion of hydrogen's effect on stress is appropriate. The conventional wisdom is that atomic hydrogen is co-deposited along with the Sn during crystal growth. The hydrogen atoms would occupy interstitial sites in the Sn crystal lattice. The as-deposited lattice parameter of the Sn would then be larger than normal. Because the equilibrium solubility of H in Sn is presumably smaller than that incorporated during plating, the H would diffuse out of the deposit after the plating process is complete. The lattice would want to contract back to its normal lattice parameter; and because it would be constrained by the substrate, would create in-plane tensile stress in the deposit. Conventional wisdom again would argue that this process would mitigate hillock and whisker formation because of a reduction in compressive stress. Our measurements, conducted within 15 min of plating but presumably after sufficient time to release hydrogen, do not show any reduction in compressive stress when samples are plated at less than full efficiency.

Pinsky [22] recently reviewed the limited work done on the effect of plating inefficiency (and presumably hydrogen evolution) on whisker propensity. Contradictory literature is cited with regard to the effect of low plating efficiency on whisker formation. For example, Lal and Moyer [23] have measured an increase from 10 to 13 µg g^{-1} H as the plating current is increased from 150 to 225 mA cm^{-2} in a methane sulfonate plating bath. Neither was especially prone to whiskers. The plating efficiency was not reported. On the other hand Jiang and Xian [24] report that the lowest electrodeposit efficiency in their study grew the most whiskers. Pinsky [22] does not describe the above mechanism of H release, but instead hypothesizes that the H affects Sn grain boundary properties and suggests that future research should examine these hypotheses.

Our results raise many questions. We have not measured the H content of our deposits. We have however shown that samples plated at low current efficiency contain higher average compressive stress yet no hillocks.

4.2 Texture

Our results for bright Sn show a distinct change in the fiber texture as the current is increased. The change in orientation is best summarized with the arrow shown in Fig. 13. In general as i/i_L increases, a transition where the (001) plane of the Sn becomes more parallel to the deposit surface is observed. Fewer hillocks are observed as the texture changes toward (001).

We do not know the reason for the change in orientation, but will examine whether this change increases or

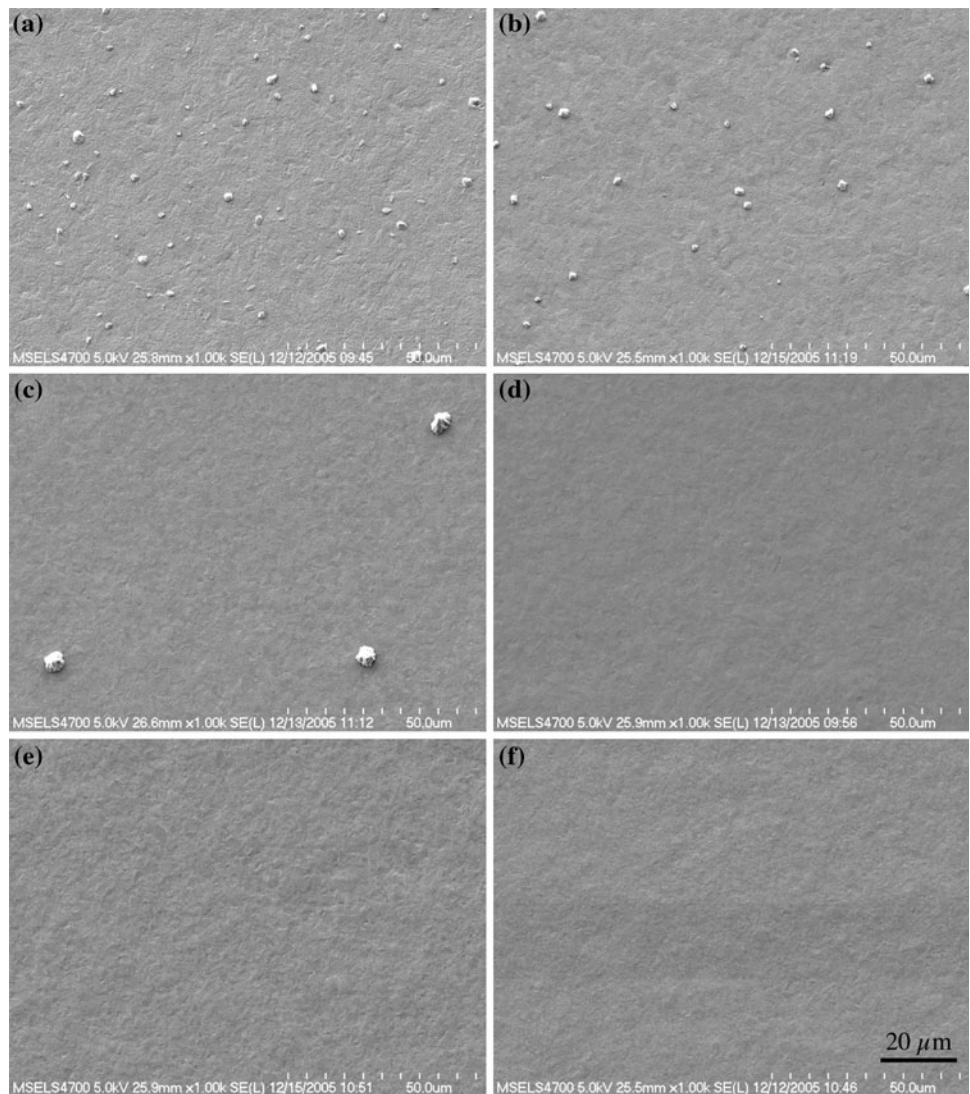

Fig. 15 Examples of SEM photos used to measure the hillock density from Exp-1: **a** 30 mA cm^{-2}, **b** 60 mA cm^{-2}, **c** 90 mA cm^{-2}, **d** 120 mA cm^{-2}, **e** 150 mA cm^{-2}, and **f** 200 mA cm^{-2}

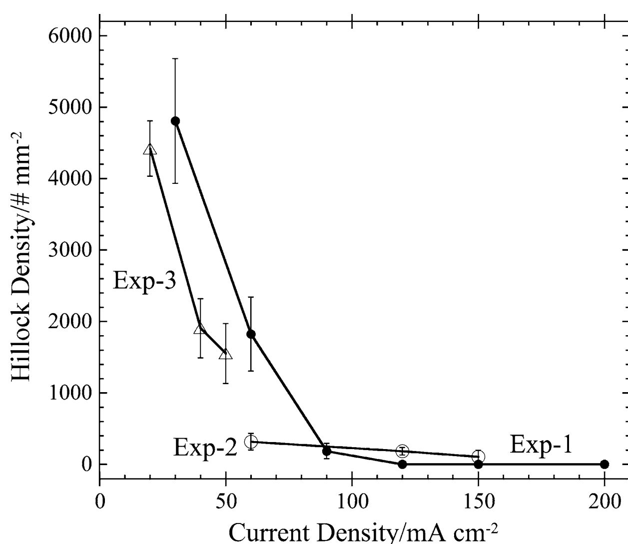

Fig. 16 Hillock density versus current density for all three data sets

decreases the likelihood of slip under a biaxial in-plane compression. Many mechanisms of stress relaxation by creep, especially at higher stresses, involve mixed diffusion and dislocation mechanisms. Furthermore, Kumar et al. [8] propose a mechanism for Sn whisker formation where compressive stress generated close to the growing intermetallic layer on the Cu/Sn interface easily reaches the yield stress of the Sn, generating dislocations that propagate to the Sn surface to be trapped there by surface oxide. This mechanism transports (spreads) the compressive stress from the interior of the deposit near the intermetallic to the surface where the whiskers can form.

The slip systems reported for Sn [15] include (110)/[001], (100)/[001], (101)/[10$\bar{1}$] and (121)/[10$\bar{1}$]. If the (001) plane were parallel to the deposit surface, the (110) and (100) planes of tetragonal Sn would be normal to the biaxial stress and there would be no shear stress on these planes in any slip direction. For a deposit with large

numbers of grains with (001) planes nearly parallel to the deposit surface, there would be fewer possible slip systems available to transport the compressive stress to the surface. In this case, the stress "spreading" mechanism of [8] would be less effective and whisker/hillock growth impeded. Such an argument may explain the absences of hillocks in our experiments at high currents.

Saito et al. [25] have examined the electrodeposition of Sn–Cu alloys on both electrodeposited and sputtered Si/Cu substrates of varying Cu thickness (0.1–8 μm). They determined from their experiments that a (001) orientation of Sn actually leads to more whiskers due to coherency stress between the Cu and the Sn. Our data under decidedly different plating conditions clearly shows that whisker (actually hillock) resistance increases as the texture rotates toward (001).

Lee et al. [4] contend that tin whiskers grow from grains whose orientation is different from the major orientation of the film. The elastic anisotropy of the Sn can cause significantly different strains in adjacent grains that can lead to oxide rupture and whisker growth at these locations. Lee calculates that the out of plane strain (ε_{33}) is 0.294 for a (100) oriented film under an 8 MPa biaxial compressive stress. The strain is significantly reduced to 0.079 for (110) and 0.069 for (001) orientations. Applying this reasoning to our stereograph of the preferred orientation in Fig. 13, the group comprised of (332), (121), and (312), deposited at low current have out of plane strains ranging from 0.08 to 0.14 whereas those grouped closer to the (001), deposited above the limiting current, fall between the much smaller range of 0.07–0.08. This would suggest that the preferred orientation of the low current deposits would lead to hillock formation whereas that of the other group would not, consistent with our experimental observations. All of these ideas require further investigation to substantiate them. It is also important that we have studied only bright Sn deposits. Results for matte Sn deposits may differ.

4.3 Grain size

The decrease in columnar grain size of deposits plated near and beyond the limiting current may provide another reason why hillock formation is suppressed in these bright Sn samples. As described in Boettinger et al. [9], the absence of grain boundaries parallel to the surface of the deposit in a columnar structure prevents the shape change of grains by a normal Coble (grain boundary) creep stress relief mechanism. Atoms of Sn must then diffuse along grain boundaries to the free surface to relieve stress, thereby making hillock (and whisker) growth likely. Indeed the role of Pb in mitigating whisker growth appears to be the breakup of the columnar structure [9]. Columnar grain structures are rarely perfect. Some grains are pinched off and overgrown by more favorably oriented grains towards the top of the deposit. Electrodeposition of extremely narrow columnar grains, as occurs at high current density in the present study, would increase the likelihood of grain pinch-off. This process could lead to some internal grain boundaries that are not perpendicular to the surface of the deposit allowing internal stress relief by normal diffusional creep of grains within the deposit and thus a mitigation of the flow of atoms and vacancies to/away from the top surface.

5 Conclusions

Electrodeposition of our bright Sn on Cu with current density above the diffusion limited current eliminates Sn hillock formation. This may be accomplished by either high current density and/or electrolyte dilution. The elimination of Sn hillocks occurs despite the fact that the Sn grains in the deposit remain columnar and the measured stress is highly compressive, features thought to promote whisker and hillock formation [9].

Changes that accompany exceeding the limiting current include a reduction in columnar grain diameter and a rotation of the preferred orientation (fiber texture) of the deposit toward the [001] direction. The smaller columnar grain diameter may increase the occurrence of pinched-off grains in the columnar structure and provide internal sinks for the grain boundary flux of atoms that would otherwise reach the surface and cause hillock growth. The change in preferred orientation makes slip on (110) and/or (100) planes unlikely. Thus the generation of dislocations is less likely and may decrease the effective spreading of compressive stress from the intermetallic region to the free surface of the deposit. Because this spreading is thought to be an important part of whisker and hillock growth [8], the orientation change may be another reason for reduced hillock formation. Our observed reduction in hillock density with change in preferred orientation is also consistent with elastic strain arguments [4] where intergranular shear due to the anisotropy of Sn is minimized when the orientation moves towards the [001]. The reason for the orientation change with decreased plating efficiency requires further investigation.

Because hillock and whisker growth are related phenomena, electrodeposition beyond the limiting current may be a possible whisker mitigation strategy.

References

1. Furuta N, Hamamura K (1969) Jpn J Appl Phys 8:1404
2. http://nepp.nasa.gov/WHISKER/index.html. Accessed 23 June 2008

3. Arnold SM (1966) Plating 53:96
4. Lee BZ, Lee DN (1998) Acta Mater 46:3701
5. Tu KN (1973) Acta Metall 21:347
6. Tu KN (1994) Phys Rev B-Condens Matter 49:2030
7. Chason E, Jadhav N, Chan WL, Reinbold L, Kumar KS (2008) Appl Phys Lett 92:171901
8. Kumar KS, Reinbold L, Bower AF, Chason E (2008) J Mater Res 23:2916–2934
9. Boettinger WJ, Johnson CE, Bendersky LA, Moon K-W, Williams ME, Stafford GR (2005) Acta Mater 53:5033–5050
10. Barsoum MW, Hoffman EN, Doherty RD, Gupta S, Zavaliangos A (2004) Phys Rev Lett 93:206104
11. Chadhari PJ (1974) Appl Phys 45:4339
12. Jackson MS, Li C-Y (1982) Acta Metall 30:1993
13. Doerner MF, Nix WD (1988) CRC Crit Rev Solid State Mater Sci 14:225
14. Bard AJ, Faulkner LR (2001) Electrochemical methods: fundamentals and applications, 2nd edn. Wiley, NJ
15. Barrett CS, Massalski TB (1980) Structure of metals crystallographic methods, principles, and data, 3rd edn. Pergamon, New York, pp 204–205
16. Chen CS, Wan CC, Wang YY (1998) Trans Inst Met Finish 76:54–58
17. Paunovic Milan, Schlesinger Mordechay (1998) Fundamentals of electrochemical deposition. Wiley, New York
18. Fleischmann M, Thirsk HR (1963) In: Delahay P, Tobias CW (eds) Advances in electrochemistry and electrochemical engineering, vol 3. Interscience, New York
19. Budevski E, Bostanov V, Staikov G (1980) Ann Rev Mater Sci 10:85–112
20. Milchev A (2002) Electrocrystallization, fundamentals of nucleation and growth. Springer, New York
21. Rashidi AM, Amadeh A (2008) Surf Coat Technol 202:3772
22. Pinsky DA (2008) Microelectron Reliab 48:105–110
23. Lal S, Moyer TD (2005) IEEE Trans Electron Packag Manuf 28:63–74
24. Jiang B, Xian A (2008) Microelectron Reliab 48:675–681
25. Saito M, Sasaki H, Katou K, Toba T, Homma T (2009) J Electrochem Soc 156:E86–E90